Establishment and Verification of the Cutting Grinding Force Model for the Disc Wheel Based on Piezoelectric Sensors

Jing Ni, Kai Feng, M.S.H. Al-Furjan * , **Xiaojiao Xu and Jing Xu**

School of Mechanical Engineering, Hangzhou Dianzi University, Hangzhou 310005, China;
nj2000@hdu.edu.cn (J.N.); fengkai319@foxmail.com (K.F.); xuxiaojiao66@foxmail.com (X.X.);
hduxujing@163.com (J.X.)
* Correspondence: rayan@hdu.edu.cn

check for updates

Abstract: In this paper, a new model of cutting grinding force for disc wheels is presented. Initially, it was proposed that the grinding cutting force was formed by the grinding force and cutting force in combination. Considering the single-grit morphology, the single-grit average grinding depth, the effective number of grits, and the contact arc length between the grit and the workpiece comprehensively, the grinding force model and the cutting force model were established, respectively. Then, a universal grinding cutting force model was optimized by introducing the effective grit coefficient model, dependent on the probability statistical method and the grit height coefficient model with Rayleigh's distribution theory. Finally, according to the different proportions of the grinding force and cutting force, the grinding cutting force model, with multi-particles, was established. Simulation and experimental results based on piezoelectric sensors showed that the proposed model could predict the intermittent grinding cutting force well. Moreover, the inclusion of the grit height coefficient and the effective grits number coefficient improved the modeling accuracy. The error between the simulation and experimental findings in grinding cutting force was reduced to 7.8% in comparison with the traditional model. In addition, the grinding cutting force can be divided into three segments; increasing, steadiness, and decreasing, respectively found through modeling.

Keywords: Grinding cutting force model; Disc Wheel; Effective grits' number; Piezoelectric sensors

1. Introduction

The grinding wheel machine is widely used in machinery, metallurgy, mining, construction, automobile manufacturing, and other industries. It is possible to cut-off non-metallic materials, metallic materials, and even parts of non-ferrous metals in high rotation speed, continuously, through this process [1]. It is known that grinding cutting is a multi-point cutting process that affects the dimensional accuracy and disc lifetime. Because of the diverse morphology of the disc wheel, the irregular distribution of grits, and the uncertainty of the number of effective grains, it is difficult for the traditional identification methods to calculate the grinding cutting force precisely, smoothly, and efficiently [2–4]. Therefore, the grinding cutting load characteristics of the grinding wheel disc in the grinding process and the calculation model of the grinding load of the grinding wheel disc with multiple grinding particles have important theoretical research value and engineering benefits for improving the machining accuracy, production efficiency, and cost involved.

At present, three types of grinding cutting force models have been put forward. The first is a physical grinding model and a numerical simulation model of single-grit. For instance, Duan et al. [5] assumed the shape of the abrasive grain to be a cone and carried out the three-dimensional grinding

simulation of the single-grit, which better solved the element distortion in the grinding simulation with the finite element method. Lang et al. [6] assumed the shape of the single-grit to be a conical shape and also assumed that the protrusion height obeyed the Rayleigh distribution, thus they derived the formula of the thickness of the undeformed abrasive chip. Su et al. [7,8] obtained the stress variation of the grits and the workpiece material by simulating a single abrasive cutting process and analyzed the wear mechanism of the grits and the grinding deformation mechanism of the workpiece material. Yan et al. [9] simulated the single-grit grinding process with the finite element method (FEM)-software AdvantEdge, established a mechanical model and numerical simulation model of a single-grit grinding under different process parameters, and verified the proposed model with scratch tests under different loads.

The second kind of grinding cutting force model is a statistical analysis of multi-particle effective grinding force. For instance, Engin et al. [10] used multiple regression analyses for circular sawing (CS) and abrasive water jet cutting (AWJC) and created a predictive chart of specific energy for the shore hardness and wear resistance. Ersoy et al. [11] successfully used statistical multivariate linear regression analysis techniques to evaluate the combined factors of the wear performance on grinding. Karakurt et al. [12] established the calculation formula of the grinding force by quoting the multi-factor statistical method and considering the grinding speed, grinding depth, and other related factors. Turchetta [13] performed a linear regression analysis on the experimental data of grinding. The results show that the radial cutting force increases with an increase in feed speed and the tangential cutting force increases with an increase in the equivalent cutting thickness. Zhang et al. [14] assumed the grits to be of a normal distribution and calculated the number of grains in the surface of the disc wheel, establishing a theoretical calculation model of the grinding force. Based on the theoretical model of the grinding force on the single-grit surface of a diamond grinding wheel, Agarwal and Rao [15,16] and Hecker et al. [17] considered the law of the protrusion height on the grit grain to be in accordance with the Rayleigh distribution and established a mathematical model for predicting the grinding force of multiple grit grains. In order to determine the actual number of grits per unit area and the number of grits per unit area engaged in grinding, Hou and Komanduri [18] proposed probabilistic methods to analyze the grinding process.

The third kind of grinding cutting force model is a simulation of multi-particle grinding forces under a complex array. Su et al. [19] proposed that all grits with the same diameter were distributed randomly and established the grinding force calculation model of a two-dimensional disc wheel. Hegeman [20] optimized the grinding process, simplified the grits into elliptic grits, and established a three-dimensional grinding wheel model. Then, simulations of the grinding force for two different materials (cemented carbide and manganese zinc ferrite) were carried out to verify the effectiveness of the cutting model. Warnecke and Barth [21] unified the grinding wheel and the workpiece into a finite element model for simulation, studied the influence of the grinding wheel vibration on material removal, and established the grinding force load calculation model. Su et al. [22] used a regular hexahedron as the basic form of grits and randomly distributed the grits on the grinding wheel to establish a grinding simulation model.

However, in the current literature, the morphology of single-grit has not been accurately considered in the establishment of the grit grinding force model. On the other hand, the number of effective grains and the unequal height arrangement of the grits on the disc wheel were also not well thought out when establishing the multi-particle grinding force model. Thus, further study is still needed to determine the multi-particle grinding cutting force model precisely. In this paper, the morphology of the grinding grit is simplified to rigid hexahedrons and a new model of multi-particle grinding cutting force is presented by considering the single-grit morphology, cutting depth, contact arc length, and number of effective grits. The simulation and experimental results with piezoelectric sensors showed that the obtained model is simple, effective, and versatile.

2. Mechanistic Model of the Cutting Grinding Force

2.1. Analysis of the Grinding Cutting Force

The grinding cutting force is a physical phenomenon caused by the contact of a grinding edge and a workpiece. Figure 1 shows the grinding cutting principle of a disc wheel, where d_s is the disc diameter, v_s is the grinding cutting speed, v_f is the feed speed, h_m is the average comprehensive grinding depth of single-grit, l_c is the contact arc length, θ is the grinding angle, l_a is the workpiece length, and l_b is the workpiece width. As shown in Figure 1, the grinding cutting force of the disc wheel includes F_X, F_y, and F_z, where F_X is the most important component. Thus, this paper mainly focuses on the horizontal grinding cutting force (F_X).
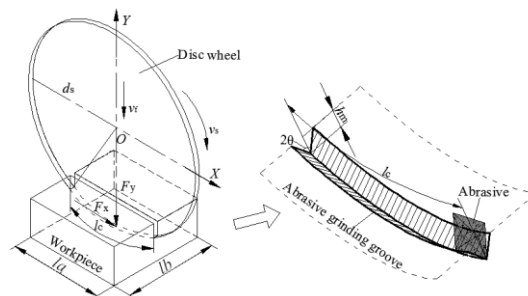

Figure 1. The grinding principle of the disc wheel.

According to hundreds of grinding cutting experiments, the following points have been identified:

(1) The grinding cutting force is formed through the combination of "grinding force" and "cutting force" and the proportions are different.

(2) The grinding force emerged through the simultaneous action of the grits; additionally, every single-grit could be regarded as a rigid polyhedron.

(3) The single-grit average grinding depths were extremely thin and different from each other.

(4) Some grits have involvement in grinding, but just above the grinding surface.

(5) The grinding force is added to the increase in the contact arc length between the grit and the workpiece.

Thus, the grinding cutting process was extremely sophisticated. In addition, the modeling process not only needed to consider the characteristics of the grinding force and cutting force, but also the grinding edge shape, the single-grit average grinding depth, the number of effective grains, and the contact arc length between the grit and the workpiece. Hence, this paper established the grinding force model (F_{X1}) and cutting force model (F_{X2}), respectively, and, according to the different proportions of the grinding force and cutting force, the grinding cutting force model with multi-particles was established.

2.2. Computational Model of the Grinding Force

As shown in Figure 1, the essence of the grinding force could be regarded as a common grinding action of many single-grits with micro edges. The grinding force (F_{X1}) could be regarded as the total sum of the single-grit grinding forces (f_{X1}) simultaneously involved in grinding on the surface of the disc wheel. Thus, the F_{X1} could be expressed as follows:

$$F_{X1} = n_e \cdot f_{X1} \tag{1}$$

where n_e is the number of effective grains in the contact arc zone and f_{X1} is the single-grit grinding force.

The single-grit grinding f_{x1} has the following relationship with the grinding area of the bilateral surface (A_g) [23]:

$$f_{X1} = k_{s1} \cdot \left(A_g \right)^{\gamma} \tag{2}$$

where k_{s1} is the specific pressure associated with the grinding material, A_g is the grinding area of a bilateral surface of the single-grit, and γ is a dimensionless constant.

According to the geometric relation of Figure 1, A_g could be expressed as:

$$A_g = \frac{h_m \cdot l_c}{\cos \theta} \qquad (3)$$

where θ is the grinding angle, h_m is the average comprehensive grinding depth of the single-grit, and l_c is the contact arc length.

Thus, after comprehensive consideration of Equations (1)–(3), the grinding force foundation model could finally be expressed as follows:

$$F_{X1} = K_{s1} \cdot \left(\frac{h_m \cdot l_c}{\cos\theta} \right)^{\gamma} \cdot n_e \qquad (4)$$

Therefore, as seen in formula (4), we obtain the exact values of θ, h_m, l_c, and n_e. Thus, the F_{X1} will be calculated.

(1)   The Model of the Grinding Angle (θ):

The grinding process is a physical phenomenon caused by the contact between the grinding edge and materials. Its essence could be regarded as the common grinding action of a large amount of single-grit with a micro edge. However, due to the diversity of the grit morphology in the surface of the disc wheel, it is difficult to calculate the grinding angle (θ) in the modeling of the grinding force characteristics. Therefore, it is necessary to simplify the grit morphology to determine the grinding angle (θ).

Figure 2 represents the grit morphology screened by ultra-deep microscope photography. As in Figure 2a, grits in the disc wheel surfaces are in an irregular arrangement with multiple edges. Fortunately, as shown in Figure 2b, most grits are a polyhedron with a clear edge contour under the observation of single-grit peeled off from the disc wheel, which looks like a hexahedron. Regardless of whether the grinding grains are tetrahedral or hexahedral, the actual sharpening edges are the corners of the grinding grain. Therefore, as in Figure 2c, the grinding grains are simplified into rigid hexahedrons and each length of hexahedron is measured and counted with many grits to determine the grinding angle (θ), as shown in Table 1. Lastly, the grinding angle is calculated using the cosine theorem (Equation (5)). The grinding angle (θ) was calculated as 36.87.

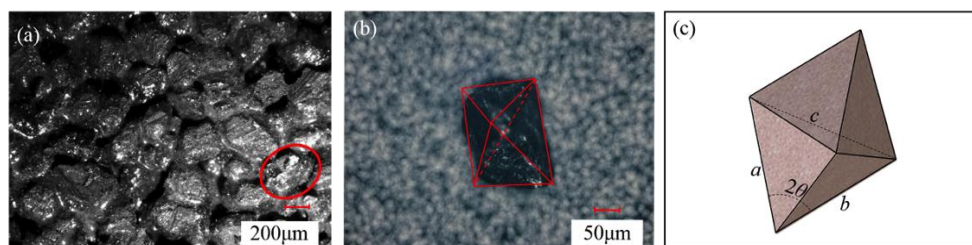$$\cos(2\theta) = \frac{a^2 + b^2 - c^2}{2ab} \qquad (5)$$

Figure 2. The principle diagram of the simplification of single-grit: (**a**) The surface of the disc wheel; (**b**) Single-grit morphology; (**c**) The single grain model.

Table 1. The size of the grit particles.

No.	a (mm)	b (mm)	c (mm)	Grinding Angle (θ (degree))
1	0.3	0.25	0.25	
2	0.25	0.3	0.35	
3	0.3	0.3	0.27	
4	0.31	0.34	0.35	
5	0.25	0.30	0.28	
6	0.34	0.36	0.37	
Average value	0.29	0.31	0.31	36.87

(2) The Model of the Comprehensive Grinding Depth of Single-grit (h_m):

Figure 3 shows the protrusion height of the grits, whereas the existing research studies have treated the single-grit average grinding depth as uniform, as shown in Figure 3b. It can be written as follows [24]:

$$h_m = \frac{18 \cdot \pi d_s v_f}{5 \cdot b_w n_t v_s}$$

(6)

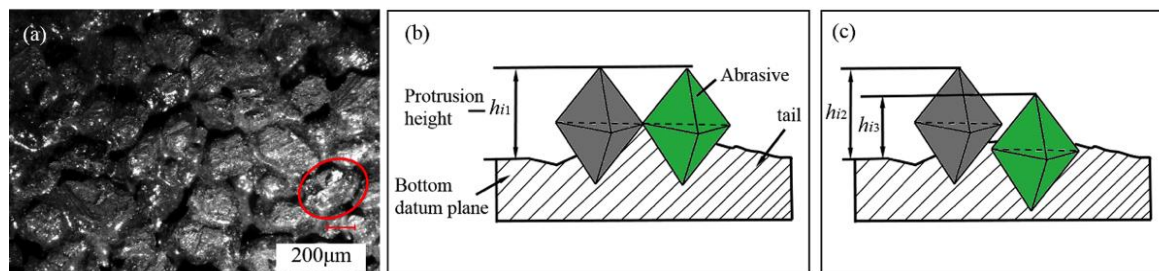where n_t is the total grinding grain number in a grinding surface and b_w is the blade thickness.

Figure 3. The protrusion height of the grits: (**a**) The surface of the disc wheel; (**b**) An equal height grit [24]; (**c**) An unequal height grit.

However, a large number of observations indicated that the grits were of uneven height on the disc surface, as shown in Figure 3c. Therefore, the above calculation has an error and it is necessary to optimize the above model. As shown in Figure 4, we found that the statistical chart of the grit protrusion height, counted with hundreds of measurements, is very similar to the probability density distribution map of Rayleigh's distribution with the observation and sampling by a microscope with depth. Therefore, the Rayleigh distribution could be used to explain the protrusion height of single-grit. Its function can be described as follows:

$$f(h) = \begin{cases} \frac{h}{\sigma^2} \cdot e^{-\frac{h^2}{2\sigma^2}} & h \geq 0 \\ 0 & h < 0 \end{cases}$$

(7)

where h is the grit protrusion height and σ is the probability density function parameter (σ = 100 μm here), as seen in Figure 4.
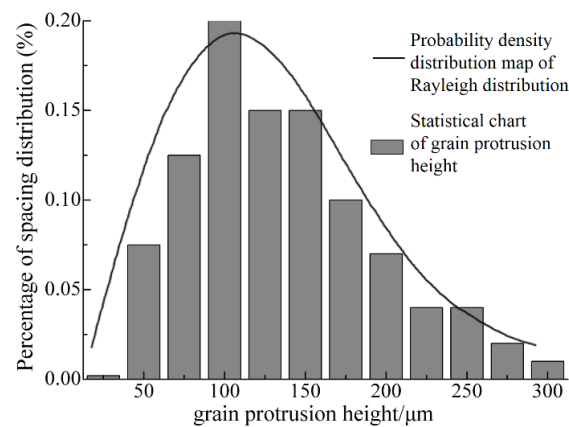
Figure 4. A diagram of the grain protrusion height.

The grit height coefficient is introduced by the Rayleigh distribution to optimize the grinding depth (h_m). As shown in Figure 4, the grain protrusion height ranges from 50 μm to 300 μm. Using the Newton-Leibniz formula and the probability density calculation, the grit height coefficient (ε) can be expressed as:

$$\varepsilon = F(h) = \int_{50}^{300} f(h)dh \tag{8}$$

where ε is the grit height coefficient.

From Equations (6) and (8), the single-grit average grinding depth (h_m) can be written as follows:

$$h_m = \varepsilon \cdot \frac{18 \cdot \pi \cdot d_s v_f}{5 \cdot b_w n_t v_s} \tag{9}$$

(3) The Model of the Contact Arc Length (l_c):

Figure 5 shows the grit trajectory and contact arc length, where β is the workpiece contact angle, a_p is the linear displacement related to the workpiece, and when the blade turns angle β, l_{c1} is the contact arc length in the initial phase with the center disc wheel at position O_1, l_{c2} is the contact arc length in the intermediate stages with the center disc wheel at position O_2, and l_{c3} is the contact arc length in the final stages with the center disc wheel at position O_3. It is assumed that grit A on the disc surface is in the beginning of the workpiece, connected with the blade. That blade is performing a feed movement in the vertical direction. In the coordinate plane XOY, the trajectory equation of grit A can be written as follows:

$$\begin{cases} x = \frac{d_s}{2} \cdot \sin \beta \\ y = \frac{d_s}{2} \cdot (1 - \cos \beta) - a_p \end{cases} \tag{10}$$

Here, a_p can be expressed as $a_p = \frac{v_f \cdot d_s}{4\pi \cdot v_s}\beta$, and the a_p value can then be substituted into Equation (10) and derived:

$$\begin{cases} dx = \frac{d_s}{2} \cdot \cos \beta d\beta \\ dy = \left(\frac{d_s}{2} \cdot \sin \beta - \frac{v_f \cdot d_s}{120 \cdot v_s} \right) d\beta \end{cases} \tag{11}$$

The differential value of the contact arc length (l_c) can be calculated by Equation (11):

$$dl_c = 2\sqrt{\frac{d_s^2}{4} + \left(\frac{v_f \times d_s}{120 \times v_s} \right)^2} \, d\beta \tag{12}$$

By integrating Equation (12), the contact arc length can be written as follows:

$$l_c = 4\sqrt{\left[\frac{d_s^2}{4} + \left(\frac{v_f \cdot d_s}{120 \cdot v_s}\right)^2\right]\left(\frac{a_p}{d_s}\right)} \tag{13}$$

Without considering the influence of the feed movement ($v_f = 0$), the contact arc between the disc wheel and the workpiece can be expressed as:

$$l_c = \begin{cases} 2 \cdot \sqrt{d_s \cdot a_p} & 0 \le a_p \le p_s \\ d_s \cdot \arcsin\frac{l_b}{d_s} & p_s \le a_p \le b \\ d_s \cdot \arcsin\frac{l_b}{d_s} - 2 \cdot \sqrt{d_s \cdot a_p} & a \le a_p \le a + p_s \end{cases} \tag{14}$$

where p_s is the depth when the disc wheel contacts the workpiece side immediately and can be expressed as:

$$p_s = \frac{d_s - \sqrt{d_s^2 - l_b^2}}{2} \tag{15}$$

Equation (15) is the contact arc length between the disc and the workpiece in the intermediate stages of the inception phase and the final stages.
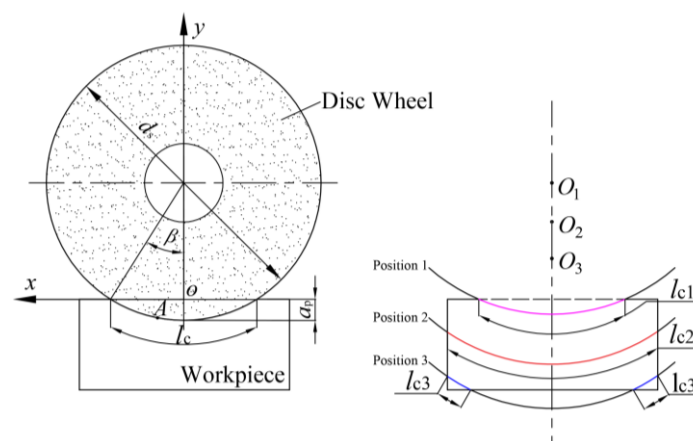

Figure 5. The motion track and contact arc length of the grits in grinding.

(4)　The Model of the Number of Effective Grains:

(a)　Computing method of the grit density:

A probability statistical method (sampling distribution) is used to calculate the grit density. Firstly, the disc surface is divided into several square areas (s_1) equally and as a whole (N). Secondly, several random regions (k), ($X_1, X_2, \ldots, X_k$), have been extracted, leaving a random sample with a capacity of K from the total N. Figure 6 shows the six different areas enlarged in the same new blade, numbered 1, 2, 3, 4, 5, and 6. Four regions in each picture ($s_1 = 4$ mm^2, $k = 24$) are selected. Thus, the grit density (ρ_s) could be expressed as:

$$\rho_s = \frac{\sum\limits_{i=1}^{k} X_k}{k \cdot s_1} \tag{16}$$

The grit density, counted by a stereomicroscope, was added up in Table 2. The quantity of the grit in every area varies from 3 to 6 and the grit density remains from 1 to 1.31. Thus, according to the calculation of Equation (16), the grit density (ρ_s) is 1.16 mm^{-2}.
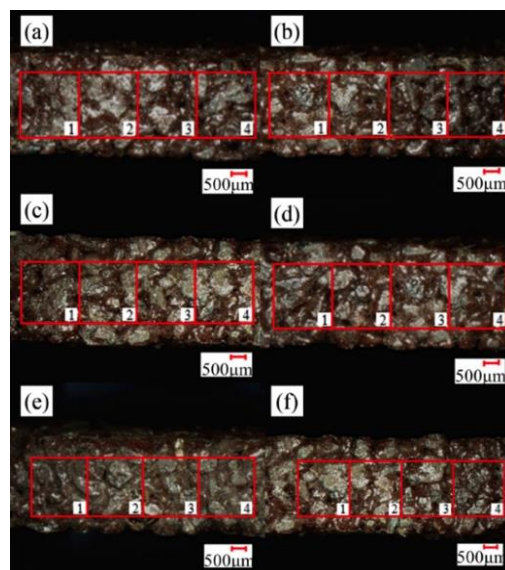
Figure 6. A microscopic amplification diagram of the grinding wheel. (**a**) Area a; (**b**) Area b; (**c**) Area c; (**d**) Area d; (**e**) Area e; (**f**) Area f.

Table 2. The grit number in the disc wheel surface.

Area	Grit Number				Average Number of Grit	Grit Density
	1	2	3	4		
a	6	5	4	6	5.25	1.31
b	4	4	5	5	4.5	1.13
c	3	5	5	5	4.5	1.13
d	6	6	5	4	5.25	1.31
e	3	4	4	6	4.25	1.06
f	5	4	3	4	4	1

(b) Computing method of the number of effective grains:

Firstly, the total number of grits (n_t) in effective contact arc areas could be expressed as:

$$n_t = l_c \times b_w \times \rho_s \tag{17}$$

Secondly, the grits in the disc surface are uneven and some grits' grinding edges were on the disc surfaces while others were embedded at a certain depth, as shown in Figure 7a. Therefore, the number of grits presented in grinding was less than that on the disc wheel surface. Additionally, it is necessary to count the actual grits involved in the grinding.

Using the analysis methods of Zhang [25], the grits on the work surface of the disc wheel are uneven. If we determined a certain penetration depth along the disc wheel radius (a_h), it could be regarded as being involved in grinding. Figure 8 shows the relationship between the penetration depths and the effective grits per unit length.
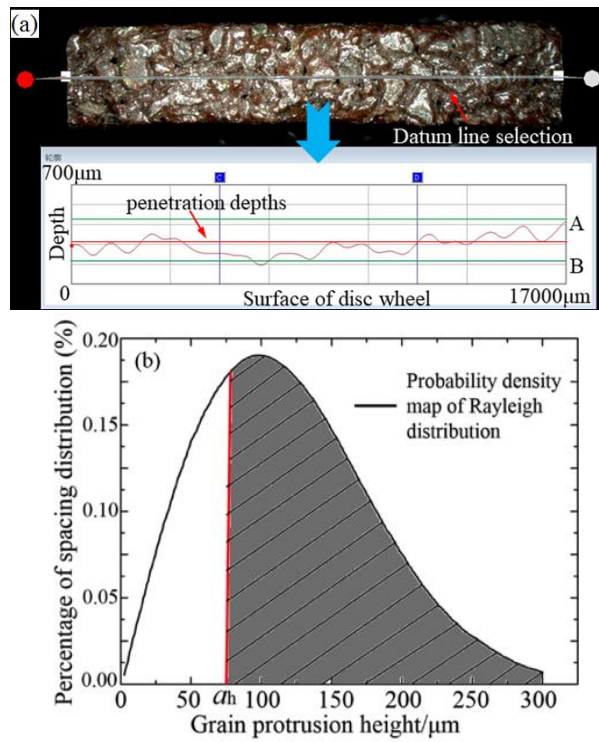
Figure 7. The bulge height distribution diagram of the surface grit particle in the grinding wheel: (**a**) The bulge height distribution diagram; (**b**) The position of the penetration depths.
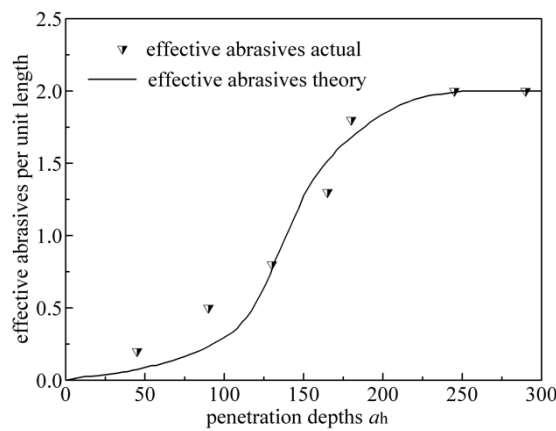

Figure 8. The relationship between the penetration depths and the effective grits per unit length [25].

As seen from Figure 8, the greater the penetration depth, the greater the number of effective grits, however, when the penetration depth increases to a certain extent, the number of grinding edges will not increase any more. Based on analysis and deduction in [25], the penetration depths can be expressed as:

$$a_h = \left[\frac{2}{C_1 K_s}\right]^{\frac{1}{p+1}} \left[\frac{v_f}{v_s}\right]^{\frac{1}{p+1}} \left[\frac{a_p}{d_{eq}}\right]^{\frac{1}{2(p+1)}} \tag{18}$$

where a_h is the penetration depth, d_{eq} is the equivalent diameter of the disc wheel, C_1 is the coefficient related to the density of the grinding edge, K_s is the coefficient related to the shape of the grinding edge, and p is the index ($p = 2$).

Figure 8 represents the probability of the density distribution map of the Rayleigh distribution and shows that a small part of the grits is not involved in grinding, with the calculation of Equation (18). Therefore, the effective number of grains can be optimized by introducing an effective grit coefficient

(η). By combining the computing method of the penetration depths, the effective grit coefficient (η) can be expressed as:

$$\eta = \int_{a_h}^{300} f(h)dh \tag{19}$$

Finally, by considering Equations (17) and (19) comprehensively, the effective number of grains (n_e) can be expressed as:

$$n_e = \eta \cdot l_c \cdot b_w \cdot \rho_s \tag{20}$$

(5)   A computational model of the multi-particle grinding force:

This yields the equations cited elsewhere (1), (9), (14), and (20). The computational model of the multi-particle grinding force can be expressed as:

$$F_{X1} = \begin{cases} k_{s1} \cdot \left(\frac{\varepsilon d_s v_f l_{c1}}{b_w n_t v_s}\right)^{\gamma} \cdot \eta \cdot n_t & 0 \le a_p \le p_s \\ k_{s1} \cdot \left(\frac{\varepsilon d_s v_f l_{c2}}{b_w n_t v_s}\right)^{\gamma} \cdot \eta \cdot n_t & p_s \le a_p \le a \\ k_{s1} \cdot \left(\frac{\varepsilon d_s v_f l_{c3}}{b_w n_t v_s}\right)^{\gamma} \cdot \eta \cdot n_t & a \le a_p \le a + p_s \end{cases} \tag{21}$$

The Equation (21) is the computational model of the multi-particle grinding force, including the grit height coefficient (ε) and the effective grit grain coefficient (η).

2.3. Computational Model of the Cutting Force

As is known from the traditional theory of cutting force [1], the cutting force in the direction of the disc wheel is related to the cross-sectional area of the chip before plastic deformation and the specific pressure of the workpiece. The model of the cutting force (F_{X2}) could be expressed as follows:

$$F_{X2} = k_{S2} \cdot A^{\beta 1} \tag{22}$$

where k_{s2} is the specific pressure associated with the grinding material, A is the grinding area of the bilateral surface, $\beta 1$ is a dimensionless constant, and A is related to the adjacent grit spacing (L) and the blade thickness (b_w).

$$A = b_w \times v_f \times \frac{2L}{v_c} \tag{23}$$

2.4. Computational Model of the Cutoff Grinding Force

Summarizing the above modeling analysis of the grinding force and cutting force, the mathematical model of the wear cutting load characteristic is as follows:

$$F_X = \alpha F_{X1} + (1 - \alpha)F_{X2} \tag{24}$$

where α is the ratio coefficient of the grinding and cutting characteristics determined by the experimental data.

Based on hundreds of actual grinding cutting test conditions, α is a parameter related to the total number of grits (n_t) and the number of effective grains (n_e) on the surface of the disc wheel. Thus, according to the numerical simulation fitting, α could be expressed as:

$$\alpha = \exp\left[-\frac{n_g}{n_t}\right] \tag{25}$$

3. Experiment

Figure 9 shows the auto-feeding grinding machine that was used in the experiment. The necessities of grits include brown alumina (GZ), 24 mesh granularity, a resin binder, a hardness rating (Y), and a

straight wheel shape. In our research, the most common material, carbon steel (Type Q235), was used as a workpiece. In order to measure the grinding force, a three-dimensional force piezoelectric sensor (ME K3D120), mounted on the table of the disc wheel with a precision of 0.1% and a measurement range of ± 1 kN, was utilized. A clamp to hold the workpiece was bolted onto the dynamometer. The grinding cutting force signal from the sensor was collected by the acquisition instrument (INV3018CT) and analyzed by the software (CIONV DASP V10). Additionally, the sampling frequency was 1 kHz. Further details of the experimental parameters are shown in Table 3. Based on the linear regression analysis and simulation results showed in the Equations (1), (19), and (20), $k_s = 0.8$, $k_{s1} = 0.92$, $k_{s2} = 1.47$, and $x = 0.3365$.
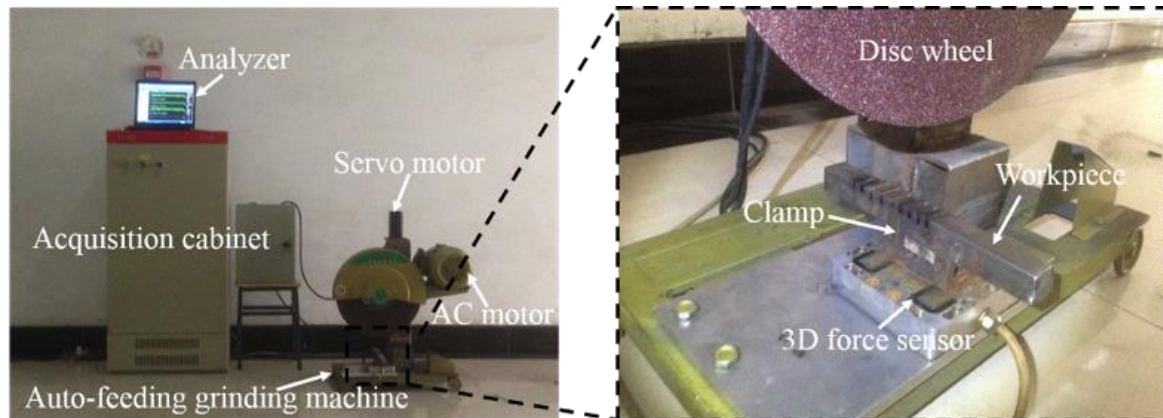

Figure 9. The experimental set-up used for the grinding tests.

Table 3. The experimental parameters.

Parameters	Value	Unit
Grinding machine power	3000	W
Rated voltage	220	V
Rated frequency	50	Hz
Blade diameter, d_s	0.4	m
Blade thickness, b_w	0.0032	m
Grinding speed, v_s	40, 45, 50, 55, 60	m/s
Feed speed, v_f	0.42, 0.83, 1.25, 1.67	$\times 10^3$ m/s
Workpiece length, l_a	0.05	m
Workpiece width, l_b	0.05	m
Workpiece height	0.02	m

4. Results and Discussion

Figure 10 shows the experimental and simulation results ($v_f = 0.42$ mm/s, $v_s = 40$ m/s).

(1) As shown in Figure 10a, in the initial phase, the grinding cutting force increased when the number of grits engaged in the grinding process increased. In the intermediate phase, the grinding cutting force remained invariable with an increase in the grinding depth (Figure 10b) because, when the grinding depth increases, the contact arc length (l_c) remains constant, and the effective number of grains remains static, as does the grinding cutting force. Figure 10c shows the final stage, whereas the grinding cutting force decreased with the increase of the grinding depth because, with the grinding depth increasing, the contact arc length (l_c) decreased and the effective number of grains decreased, as well as the grinding force.

(2) On one hand, if we don't consider the grit height, the coefficient ε would improve the model error. This is because the grits in the grinding area are of unequal distribution and the average comprehensive grinding depth of single-grit h_m is not identical. A conclusion that the grain protrusion height had a large influence on establishing the grinding cutting force calculation model could be

drawn. The maximum difference of error between the experiment and simulation was 20%, while the average relative error was 13.6%. On the other hand, it could improve the accuracy of the grinding cutting force model by considering the effective grit coefficient (η). The maximum difference of error between the experiment and simulation was 15.6% and the average relative error was 13%. The reason for this is that some grains were edged on the disc surface, while others were embedded at a certain depth, which means that the actual number of grinding particles involved in grinding was less than the grits in the disc surface. As shown in Figure 10, the model considering the grit height coefficient (ε) and the effective grit coefficient (η) had the best agreement with the experimental results. The maximum relative error between the simulation and the experiment was 10% and the average relative error was 7.8%. The main reasons for the error were the following two points: Firstly, due to the non-linear vibration of the machine, the experiment had some deviation and the grinding cutting force became larger. Secondly, the increasing of the chip increased the grinding cutting force during the grinding process. Above all, the conclusion may be drawn that considering the grit height coefficient (ε) and the effective grit coefficient (η) could improve the calculation accuracy.
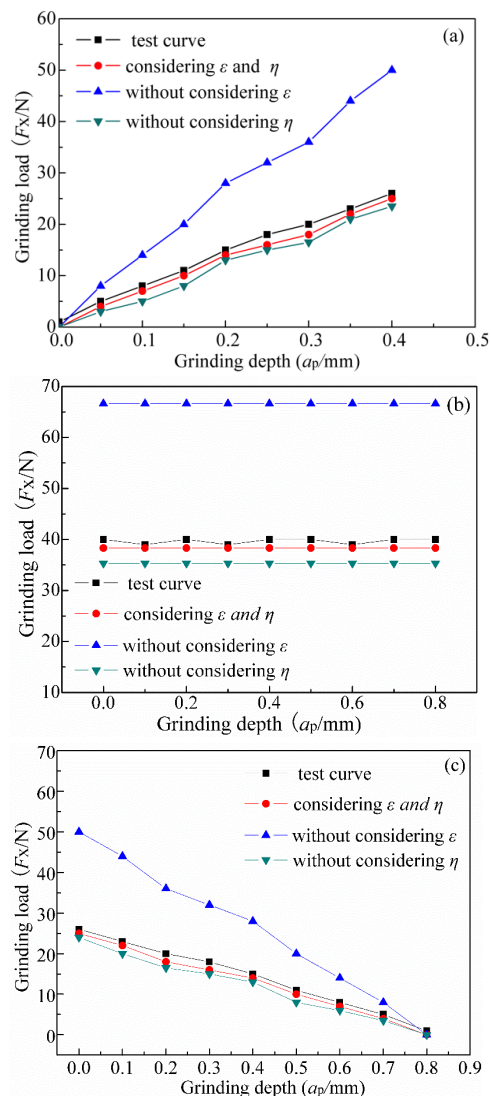

Figure 10. The simulation and experimental horizontal grinding cutting force (F_x): (**a**) Initial stage; (**b**) Intermediary stage; (**c**) Final stage. ε = the grit height coefficient and η = the effective grit coefficient.

5. Conclusions

(1) Proposing that the grinding cutting force is formed by a grinding force and a cutting force simplified the grits as rigid polyhedrons, introduced the grit height coefficient, and combined the contact arc length. This paper proposed and optimized the basic model of the grinding cutting force and reduced the simulation error by 10%.

(2) Based on the probability statistical method, which induced the effective grit coefficient and considered the number of effective grains synthetically, this paper established the multi-particles grinding cutting force calculation model and reduced the simulation error by 5.6%.

(3) The simulation and experimental results showed that it could be more precise to establish the multi-particles grinding cutting force calculation model by considering the grit height coefficient and the effective grit coefficient. The simulation and experimental error was not more than 7.8%. Therefore, the model precisely reflected the actual grinding process and provided good theoretical support of technical guidance for the optimization of the process.

Nomenclature

F_X	Cutoff grinding force
F_{X1}	Grinding force
F_{X2}	Cutting force
f_{X1}	Single-grit grinding force
h_m	The average comprehensive grinding depth of single-grit
l_c	The contact arc length
θ	Grinding angle
α	Ratio coefficient of grinding and cutting
v_f	Feed speed
v_s	Grinding cutting speed
n_e	Effective grain number
n_t	Total grinding grain number
A_g	Bilateral surface
b_w	Blade thickness
h	Grit protrusion height
σ	Probability density function parameter
ε	Grit height coefficient
a_h	Penetration depths
d_{eq}	Equivalent diameter
C_1	Coefficient related to the density of grinding edge
K_s	Specific pressure associated with grinding material
k_{s2}	Specific pressure associated with cutting material
$\beta 1$	Dimensionless constant

References

1. Li, B.; Zhao, B. *Modern Grinding Technology*; China Machine Press: Beijing, China, 2003.
2. Klocke, F.; Wrobel, C.; Rasim, M.; Mattfeld, P. Approach of characterization of the grinding wheel topography as a contribution to the energy modelling of grinding processes. *Procedia Cirp* **2016**, *46*, 631–635. [CrossRef]

3.	Li, H.N.; Axinte, D. Textured grinding wheels: A review. *Int. J. Mach. Tools Manuf.* **2016**, *109*, 8–35. [CrossRef]

4.	Matsuo, T.; Nakayama, K.; Tsukamoto, K. Machining of grinding wheel with carbide cutting tools. *Cirp Ann.-Manuf. Technol.* **1984**, *33*, 39–42. [CrossRef]

5.	Duan, N.; Wang, W.; Yu, Y.; Huang, H.; Xu, X. Dynamic simulation of single grain cutting of glass by coupling fem and sph. *China Mech. Eng.* **2013**, *24*, 2716–2721.

6.	Lang, X.; He, Y.; Tang, J.; Chen, H. Grinding force model based on prominent height of abrasive submitted to rayleigh distribution. *J. Cent. South Univ. (Sci. Technol.)* **2014**, *45*, 3386–3391.

7.	Su, C.; Hou, J.-M.; Zhu, L.-D.; Wang, W.-S. Simulation study of single grain cutting based on fluid-solid-interaction method. *J. Syst. Simul.* **2008**, *19*, 5250.

8.	Su, C.; Xu, L.; Liu, Y.; Ma, J. Numerical simulation of cutting process of cbn grit based on sph method. *Zhongguo Jixie Gongcheng (China Mech. Eng.)* **2013**, *24*, 667–670.

9.	Yan, L.; Jiang, F.; Rong, Y. Grinding mechanism based on single grain cutting simulation. *Jixie Gongcheng Xuebao (Chin. J. Mech. Eng.)* **2012**, *48*, 172–182. [CrossRef]

10.	Engin, I.C.; Bayram, F.; Yasitli, N.E. Experimental and statistical evaluation of cutting methods in relation to specific energy and rock properties. *Rock Mech. Rock Eng.* **2013**, *46*, 755–766. [CrossRef]

11.	Ersoy, A.; Buyuksagic, S.; Atici, U. Wear characteristics of circular diamond saws in the cutting of different hard abrasive rocks. *Wear* **2005**, *258*, 1422–1436. [CrossRef]

12.	Karakurt, I.; Aydin, G.; Aydiner, K. Experimental and statistical analysis of cutting force acting on diamond sawblade in sawing of granitic rocks. *Proc. Inst. Mech. Eng. Part B J. Eng. Manuf.* **2013**, *227*, 286–300. [CrossRef]

13.	Turchetta, S. Cutting force in stone machining by diamond disk. *Adv. Mater. Sci. Eng.* **2010**, *2010*. [CrossRef]

14.	Zhang, J.; Ge, P.; Zhang, L. Research on the grinding force based on the probability statistics. *Zhongguo Jixie Gongcheng/China Mech. Eng.* **2007**, *18*, 2399–2402.

15.	Agarwal, S.; Rao, P.V. A probabilistic approach to predict surface roughness in ceramic grinding. *Int. J. Mach. Tools Manuf.* **2005**, *45*, 609–616. [CrossRef]

16.	Agarwal, S.; Rao, P.V. Predictive modeling of force and power based on a new analytical undeformed chip thickness model in ceramic grinding. *Int. J. Mach. Tools Manuf.* **2013**, *65*, 68–78. [CrossRef]

17.	Hecker, R.L.; Liang, S.Y.; Wu, X.J.; Xia, P.; Jin, D.G.W. Grinding force and power modeling based on chip thickness analysis. *Int. J. Adv. Manuf. Technol.* **2007**, *33*, 449–459. [CrossRef]

18.	Hou, Z.B.; Komanduri, R. On the mechanics of the grinding process–part I. Stochastic nature of the grinding process. *Int. J. Mach. Tools Manuf.* **2003**, *43*, 1579–1593. [CrossRef]

19.	Su, C.; Xu, L.; Li, M.; Ma, J. Study on modeling and cutting simulation of abrasive grains. *Acta Aeronaut. Astronaut. Sin.* **2012**, *33*, 2130–2135.

20.	Hegeman, J. *Fundamentals of Grinding: Surface Conditions of Ground Materials*; University of Groningen: Groningen, The Netherlands, 2000.

21.	Warnecke, G.; Barth, C. Optimization of the dynamic behavior of grinding wheels for grinding of hard and brittle materials using the finite element method. *Cirp Ann.-Manuf. Technol.* **1999**, *48*, 261–264. [CrossRef]

22.	Su, C.; Yang, J.; Zhao, H.; Wang, W. Development of virtual grinding wheel and its grinding performance analysis. *J. Comput.-Aided Des. Comput. Graph.* **2008**, *20*, 560–564.

23.	Li, Y. Mechanisms and Techniques for Deep Sawing of Granite. Ph.D. Thesis, Huaqiao University, Quanzhou, China, 2004.

24.	Konstanty, J. Theoretical analysis of stone sawing with diamonds. *J. Mater. Process. Technol.* **2002**, *123*, 146–154. [CrossRef]

25.	Zhang, Y. *Metal Cutting Theory*; Aviation Industry Press: Beijing, China, 1988.